Unstable normal modes of low T/W dynamical instabilities in differentially rotating stars

Motoyuki Saijo[1,*] and Shin'ichirou Yoshida[2,†]

[1] *Department of Science, Waseda University, Shinjuku, Tokyo 169-8050, Japan*[‡]
[2] *Graduate School of Arts and Science, The University of Tokyo, Meguro, Tokyo 153-8902, Japan*

(Received 26 January 2016; Revised 3 July 2016; Accepted 2 October 2016)

We investigate the nature of low T/W dynamical instabilities in differentially rotating stars by means of linear perturbation. Here, T and W represent rotational kinetic energy and the gravitational binding energy of the star. This is the first attempt to investigate low T/W dynamical instabilities as a complete set of the eigenvalue problem. Our equilibrium configuration has "constant" specific angular momentum distribution, which potentially contains a singular solution in the perturbed enthalpy at corotation radius in linear perturbation. We find the unstable normal modes of differentially rotating stars by solving the eigenvalue problem along the equatorial plane of the star, imposing the regularity condition on the center and the vanished enthalpy at the oscillating equatorial surface. We find that the existing pulsation modes become unstable due to the existence of the corotation radius inside the star. The feature of the unstable mode eigenfrequency and its eigenfunction in the linear analysis roughly agrees with that in three-dimensional hydrodynamical simulations in Newtonian gravity. Therefore, our normal mode analysis in the equatorial motion proves valid to find the unstable equilibrium stars efficiently. Moreover, the nature of the eigenfunction that oscillates between corotation and the surface radius for unstable stars requires reinterpretation of the pulsation modes in differentially rotating stars.

PACS numbers: 04.25.Nx, 04.40.b, 97.10.Kc, 97.10.Sj

arXiv:1610.05328v1 [astro-ph.SR] 17 Oct 2016

I. INTRODUCTION

Low T/W dynamical instability in differentially rotating stars was first discovered by numerical simulations [1–5]. Here, T and W represent rotational kinetic energy and gravitational binding energy of the star. The instability timescale is dynamical, and the spiral- and bar-type deformation is found, but the strength of instability seems weaker than the standard dynamical bar instability [6–8]. Since low T/W dynamical instability takes place in a simple physical system of self-gravitating differentially rotating objects, it is considered as playing an essential role in many astrophysical scenarios of compact objects. Mergers of binary neutron stars may form differentially rotating objects and trigger a spiral type of low T/W dynamical instabilities [9, 10]. A spiral type of low T/W dynamical instabilities may play an essential role in supernova explosion for efficient angular momentum transport after the core bounce, e.g., Ref. [11]. The effect of fragmentation of the star may be caused by the low T/W dynamical instabilities [12–14]. In all these scenarios, nonaxisymmetric deformation of the compact objects arises due to low T/W dynamical instabilities, and it generates gravitational waves that are to be detected in the ground-based or the space-based interferometer within next five years [15].

Among the variety of astrophysical applications of low T/W dynamical instabilities, its mechanism is still unknown. There are several studies on corotation instabilities along the cylindrical star [16] or along the accretion disk system with Wentzel-Kramers-Brillouin (WKB) approximation [17, 18]. There is an indication from the basic pulsation equations that the corotation radius (the radius where the equilibrium fluid and pattern rotate at the same angular speed) inside the star may play a role for low T/W dynamical instabilities [19]. For the rotating stellar configuration, Saijo and Yoshida [20] investigate in practice the instabilities using the canonical angular momentum by both hydrodynamical and perturbative approaches and find that the corotation radius plays an essential role for angular momentum transport (see also Ref. [21]). Recently, properties of the f mode have been studied when corotation exists inside the stars in the linearized Newtonian hydrodynamics [22].

In this paper, we focus on the nature of low T/W dynamical instabilities mainly from the normal mode analysis in the equatorial motion of the star by the linear perturbation approach. Our particular concern is the investigation of the stability and its nature of the system with eigenvalue analysis. We introduce a simplified one-dimensional eigenvalue problem in the equatorial motion, with taking possible corotation singularity in perturbed enthalpy into account (see also Ref. [18] for corotation singularity in accretion disk system). Although there is a study that existing f mode is unstabilized when high degree of differential rotation is taken into account [3, 4] or corotation occurs [22], we never ascertain whether corotation singularity generates new types of pulsation modes in differentially rotating stars without examining the complete set of eigenmode analysis. Full

* E-mail: saijo@aoni.waseda.jp
† E-mail: yoshida@ea.c.u-tokyo.ac.jp
‡ Present address: Department of Physics, Waseda University, Shinjuku, Tokyo 169-8555, Japan

two-dimensional studies of linear eigenmodes of rapidly rotating stars have been done mainly in the uniformly rotating stars, e.g., Refs. [23, 24]. The effect of differential rotation is considered [3, 4, 25–27], but the detailed examination of relation between corotation singularity and the excitation of low T/W dynamical instability remains beyond their study. Therefore, we simply focus on the equatorial motion, which can easily handle corotation singularity. We then investigate the nature of the eigenfunction of the mode from the viewpoint of the existence of corotation inside the stars. Finally, comparison of our eigenmode analysis in the perturbative approach with those in three-dimensional hydrodynamics clearly shows that our model contains sufficient valid physics. Throughout this paper, we use gravitational units with $G = 1$.

II. LINEAR PERTURBATION

Axisymmetric equilibrium configuration of differentially rotating stars in Newtonian gravity can be constructed numerically by using the technique established by Hachisu [28, 29]. We impose perfect fluid with a polytropic equation of state $p = \kappa\rho^{\Gamma}$, where p is the pressure, ρ is the rest mass density, κ is the constant, $\Gamma = 1 + 1/n$ is the adiabatic exponent, n is the polytropic index, and j-constant rotation law for the angular velocity distribution is

$$\Omega = \frac{j_0}{d^2 + \varpi^2},$$

where j_0 is the constant, d is the degree of differential rotation, and ϖ is the radial distance of the cylindrical coordinates. Here, we focus on the low T/W dynamically unstable star, which is summarized in Table I. Note that models I and II represent $m = 2$ and $m = 1$ dominant dynamically unstable stars.

We perturb the differentially rotating stars nonaxisymmetrically in order to investigate the feature of low T/W dynamical instabilities. The nonaxisymmetrically perturbed quantity δq has a dependence of $\delta q = \delta q_m(\varpi, z)e^{-i\omega t+im\varphi}$, where z is the coordinate along the rotational axes and φ is the azimuthal coordinate.

We impose one assumption in which the equatorial motion of the perturbed quantities alone is taken into account. Our basic idea is that the characteristic wave propagation due to rotation mainly lies in the equatorial plane. The pulsation equations of differentially rotating stars in Newtonian gravity in the equatorial motion can be written by using the perturbed continuity equation, perturbed Euler equation and perturbed Poisson equation as (e.g., Ref. [18])

$$\left[\frac{d^2}{d\varpi^2} - \left(\frac{d}{d\varpi}\ln\frac{D}{\rho\varpi}\right)\frac{d}{d\varpi} - \frac{2m\Omega}{\varpi\tilde{\omega}}\left(\frac{d}{d\varpi}\ln\frac{\rho\Omega}{D}\right) - \frac{m^2}{\varpi^2} - \frac{D}{dp/d\rho}\right]\delta U_m(\varpi) = -\frac{D}{dp/d\rho}\delta\Phi_m(\varpi), \quad (1)$$

$$\left[\frac{d^2}{d\varpi^2} + \frac{1}{\varpi}\frac{d}{d\varpi} - \frac{m^2}{\varpi^2} + 4\pi\rho\frac{d\rho}{dp}\right]\delta\Phi_m(\varpi) = 4\pi\rho\frac{d\rho}{dp}\delta U_m(\varpi), \quad (2)$$

where δU_m is the scalar potential $\delta U_m \equiv \delta h_m + \delta\Phi_m$, δh_m is the perturbed enthalpy, and $\delta\Phi_m$ is the perturbed gravitational potential; $D = \kappa^2 - \tilde{\omega}^2$, with κ^2 being $\varpi(d\Omega^2/d\varpi) + 4\Omega^2$ and $\tilde{\omega} = \omega - m\Omega$. Note that we discard the second-order z derivative in δU_m and $\delta\Phi_m$ (the first-order z derivative in δU_m and $\delta\Phi_m$ automatically disappears due to the equatorial symmetry we imposed in the system) to derive Eqs. (1) and (2). The equations contain singular solution around $\tilde{\omega} = 0$. Expanding the equations around the corotation radius (the radius $r_{\rm cr}$ where $\omega = m\Omega$ in a pure real frequency), we can easily find the singular solution in δU_m as

$$\delta U_m = A_{1m}x + A_{2m}\big[1 + |\beta|x(-1 + 2\gamma + \log|\beta| + \log|x|) + O(x^2)\big], \quad (3)$$

$$\beta = -\frac{2\Omega_{\rm cr}}{r_{\rm cr}d\Omega/d\varpi|_{\varpi=r_{\rm cr}}}\left.\frac{d}{d\varpi}\left(\ln\frac{\kappa^2}{\rho\Omega}\right)\right|_{r=r_{\rm cr}} < 0, \quad (4)$$

where $x \equiv \varpi - r_{\rm cr}$, A_{1m} and A_{2m} are constants, γ is the Euler's constant, and $\Omega_{\rm cr}$ is the angular velocity at corotation. Since δU_m contains the term $x\log|x|$, $d\delta U_m/d\varpi$ contains singular behavior at corotation. To construct a solution across corotation in a pure real frequency ($\Im[\omega] = 0$), analytic continuation is necessary on corotation. Since $\delta\Phi_m$ is regular from the fact that δU_m is continuous on the corotation [see Eq. (2)], only the singular behavior (discontinuity in the first derivative of δU_m) is contained in δh_m.

To check our assumption, we compare the results of linear perturbation in the cylindrical model with those of hydrodynamics in Sec. IV.

TABLE I. Equilibrium configuration of differentially rotating stars

Model	n	r_p/r_e [a]	Ω_c/Ω_e [b]	T/W
I	1	0.625	26.0	6.09×10^{-2}
II	3	0.625	26.0	7.21×10^{-2}

[a] r_p: Polar surface radius; r_e: Equatorial surface radius
[b] Ω_c: Central angular velocity; Ω_e: Equatorial surface angular velocity

III. UNSTABLE NORMAL MODES

We study the stability of the system by introducing eigenvalue problem. We impose regularity conditions at the center as

$$\delta U_m = C_{1m}\varpi^{|m|}, \qquad \delta\Phi_m = C_{2m}\varpi^{|m|},$$

where C_{1m} and C_{2m} are constants. We set the boundary condition for $\delta\Phi_m$ at infinity as the quantity is finite ($\delta\Phi_m \propto \varpi^{-|m|}$). This is equivalent to imposing a surface boundary condition as $\delta\Phi_m = C_{3m}\varpi^{-|m|}$. The constant C_{3m} is described by an appropriate combination of C_{1m} and C_{2m}, which is determined from the condition that $\delta\Phi_m$ and $d\delta\Phi_m/d\varpi$ are continuous across the surface. We also impose the surface boundary condition for δU_m as the enthalpy vanishes on the oscillating surface of the stars. Namely

$$\delta h_m + \xi^j_m \nabla_j h = 0, \tag{5}$$

where ξ^i_m is the Lagrangian displacement [30], ∇_j is the covariant derivative, and h is the equilibrium enthalpy. Only 1 degree of freedom seems to remain in the system, which represents the normalization factor. We set $C_{1m} = 1$ in our computational code.

The axisymmetric equilibrium configuration of the differentially rotating stars is computed in the two-dimensional cylindrical coordinates [29]. Then we take the equilibrium quantities q ($\equiv p/\rho$) and Φ (gravitational potential) 3841 grid points along the equatorial plane from the center to the stellar surface in order to integrate the pulsation equations. We apply a fourth-order Runge-Kutta method to integrate Eqs. (1) and (2).

We search a complex frequency ω in the region of $\Re[\omega] \in [0, m+0.4]\ \Omega_c$ and $\Im[\omega] \in [0, 0.1]\ \Omega_c$, with nondimensional resolution $\Delta\omega/\Omega_c = 1 \times 10^{-5}$ for both real and imaginary frequencies. Introducing a complex frequency ω avoids singular solution at corotation ($\tilde{\omega} \neq 0$ for $\Im[\omega] \neq 0$ inside the star). We integrate Eqs. (1) and (2) from the center to the half-radius, and from the surface with boundary conditions including Eq. (5) to the half-radius, and then match the solutions by computing the determinant, composed of two sets of solutions δU_m, $d\delta U_m/d\varpi$, $\delta\Phi_m$ and $d\delta\Phi_m/d\varpi$. Only a successful choice of frequency can generate the solution from the center to the surface. We determine the eigenfrequency when the absolute value of the determinant takes the minimum at a

TABLE II. $m = 1$ and $m = 2$ normal modes of differentially rotating stars in the cylindrical model

Model	m	N[a]	$\Re[\omega]/\Omega_c$	$\Im[\omega]/\Omega_c$	$r_{\rm cr}/r_e$[b]
I	1	1	0.65275	0.00012	0.14587
I	1	2	1.15197	0.00000	···
I	2	0	0.29017	0.00855	0.48549
I	2	1	0.89791	0.00100	0.22158
I	2	2	1.39597	0.00039	0.13156
I	2	3	1.86074	0.00024	0.05471
I	2	4	2.31080	0.00000	···
II	1	0	0.52603	0.05126	0.18985
II	1	1	0.72759	0.00688	0.12238
II	1	2	0.97965	0.00011	0.02883
II	1	3	1.24636	0.00000	···
II	2	0	0.52656	0.00041	0.33456
II	2	1	0.71208	0.00147	0.26897
II	2	2	0.94196	0.00072	0.21197
II	2	3	1.17403	0.00039	0.16775
II	2	4	1.40432	0.00037	0.13026
II	2	5	1.63112	0.00038	0.09511
II	2	6	1.85820	0.00046	0.05525
II	2	7	2.08739	0.00000	···

[a] N: Node numbers between the corotation and surface radius
[b] $r_{\rm cr}$: Corotation radius (the radius where $\Re[\omega] = m\Omega$)

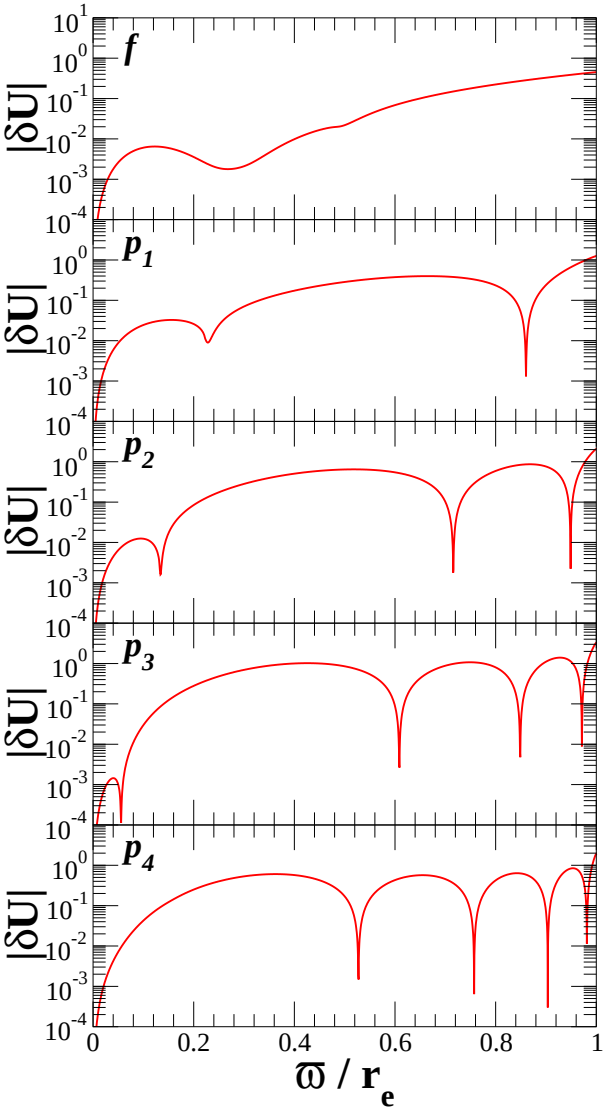

FIG. 1. Eigenfunctions of the first five $m = 2$ normal modes of differentially rotating $n = 1$ polytropic stars in the cylindrical model. Labels f and p_N denote the f mode and p modes with node number N in Table II, respectively. Note that node numbers counted between corotation ($r_{\rm cr}/r_e = 0.486, 0.222, 0.132, 0.0564$ for $N = 0$, 1, 2, 3 normal modes) and the equatorial surface radius are used to identify f and p modes.

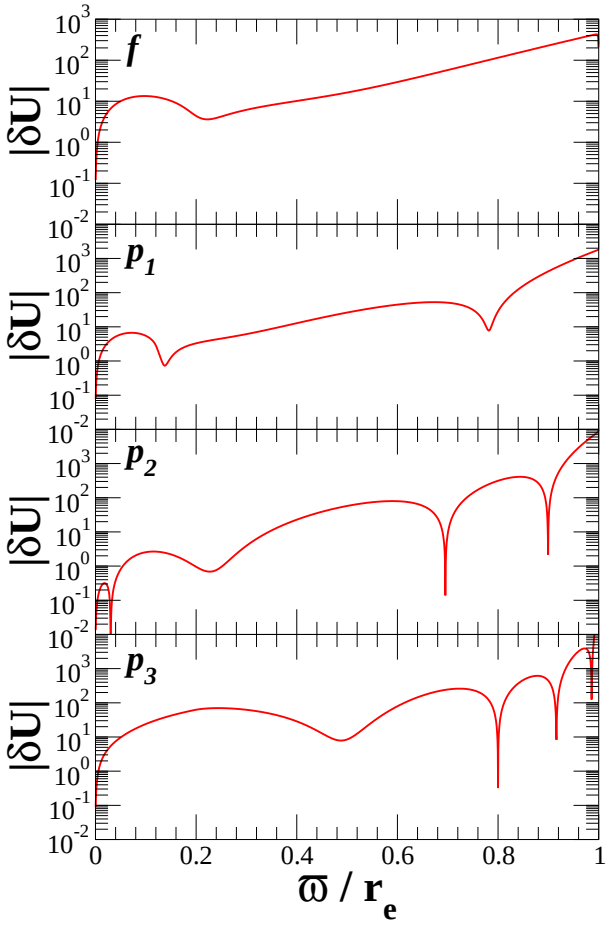

FIG. 2. Same as Fig. 1, but for first three $m = 1$ normal modes of $n = 3$ polytropic stars. Note that the corotation radius for $N = 0$, 1, and 2 normal modes are $r_{\rm cr}/r_e = 0.190$, 0.122, and 0.0288.

certain complex frequency by comparing with that at the neighbouring four frequencies in the complex frequency plane. Since our approach cannot treat $\tilde{\omega} = 0$ inside the star due to corotation singularity, we simply discard the search region $\Re[\omega] \in [0, m]\ \Omega_c$ and $\Im[\omega] \in [0, 0.2\ \Delta\varpi/r_e]\ \Omega_c$, where the nondimensional grid resolution $\Delta\varpi/r_e \equiv 1/3840 \approx 2.6 \times 10^{-4}$. Note that $\omega/\Omega_c = 0.2\ \Delta\varpi/r_e$ is a typical angular momentum resolution around the surface ($\Delta\Omega/\Omega_c \gtrsim \Delta\Omega_e/\Omega_c \approx 7.4\times10^{-2}\Delta\varpi/r_e$ for $\Omega_c/\Omega_e = 26$). Here, we only focus on $m = 1$ spiral and $m = 2$ bar modes.

We show the series of the complex eigenfunction in Fig. 1 for the $m = 2$ mode of model I and in Fig. 2 for the $m = 1$ mode of model II. All the first five nodes for $m = 2$ and the first three for $m = 1$ can be seen along the radial direction in each eigenfunction. For example, the fundamental unstable mode ($N = 0$ in Table II) has no node (the eigenfunction does not cross zero), which represents the f mode (e.g., Ref. [31]). The other unstable modes in Table II have N nodes, i.e. the eigenfunctions cross zero N times between the corotation and surface radius. The features can be interpreted to mean that these modes are p modes (e.g., Ref. [31]). The reason for counting the node numbers between the corotation and surface radius is to reckon the strength of the corotation barrier to each eigenfunction. An unstable eigenfunction has a sharp change at the corotation radius, since the corotation singularity acts as a potential barrier for wave propagation. The sharp change in the eigenfunction can also be interpreted as a phase gap in the eigenfunction, which arises through analytic continuation on corotation. We summarize our results of complex eigenfrequencies in Table II. We only find the known types of modes (f and p modes) with every node numbers are present in our analysis of the equatorial fluid motion, except for the f mode ($N = 0$) in model I. Note that we discard the "eigenfrequency" which relates to a constant cylindrical displacement [32]. Also all eigenfrequencies which possess corotation inside the star are found unstable. The dominance of the $m = 1$ or $m = 2$ mode depends on the stiffness of the equation of state. In fact, the shortest timescale $\tau \equiv (\Im[\omega])^{-1}$ (largest growth rate) from the normal mode analysis for model I is the case $m = 2$ f mode, while for model II, it is the case $m = 1$ f mode. This feature has also been found in numerical simulations [5, 20].

IV. COMPARISON WITH HYDRODYNAMICAL SIMULATION

We briefly introduce our three-dimensional hydrodynamical simulation in Newtonian gravity and compare the results with the linear analysis. We compute the same differentially rotating equilibrium stars summarized in Table I and impose nonaxisymmetric perturbation in the rest mass density as

$$\rho = \sum_{k=1}^{4} \rho_{\rm eq} \left[1 + \delta_k \frac{\varpi}{r_e} (\cos k\varphi + \sin k\varphi) \right],$$

where we set $\delta_i = 5 \times 10^{-5}$ $(i = 1, \cdots, 4)$ for evolution. Note that $\rho_{\rm eq}$ is the equilibrium configuration of the rest mass density, x and y are the components of Cartesian coordinates, and the cylindrical radius ϖ is $\varpi = \sqrt{x^2 + y^2}$. We insert the approximate Harten-Lax-van Leer (HLL) Riemann solver [33] with the same reconstruction method, MC-limiter [34], for hydrodynamics in our code [29]. We have demonstrated the results of the wall shock problem in our code, which are in full agreement with those of one-dimensional analytical solution. We monitor the diagnostics M_1 and M_2 (e.g., Ref. [29]), which are the $m = 1$ and $m = 2$ rest mass density-weighted average in the whole volume, and find that both M_1 and M_2 grow exponentially in time for low T/W dynamically unstable case. Here we focus on the dominant m mode for each model (Table I). In practice, the diagnostic M_2 grows exponentially up to $t \approx 170\ P_c$ for model I and M_1 to $t \approx 70\ P_c$ for model II, and sat-

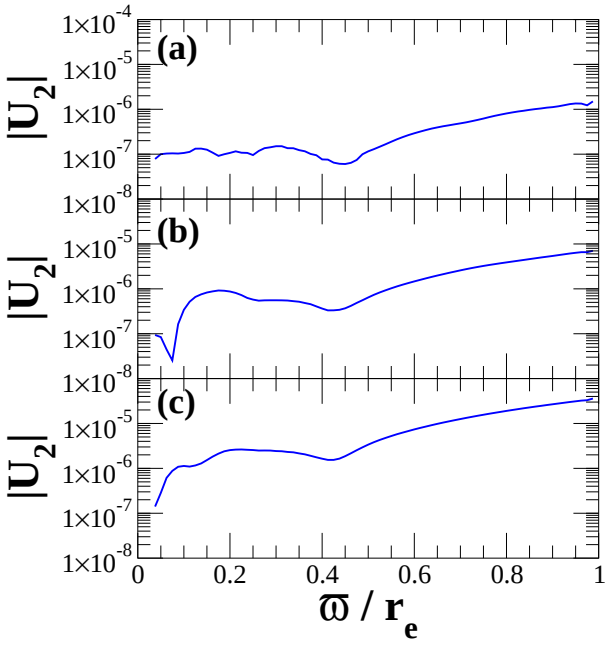

FIG. 3. The $m = 2$ scalar potential density diagnostics in the equatorial plane. Note that U_2 represents the $m = 2$ scalar potential density weighted average in the equatorial plane. The labels (a), (b), and (c) denote the evolution time $t = 59.7\ P_c$, $74.6\ P_c$, and $89.5\ P_c$, respectively. We find features similar to the cylindrical model (Fig. 1) in which no nodes are present.

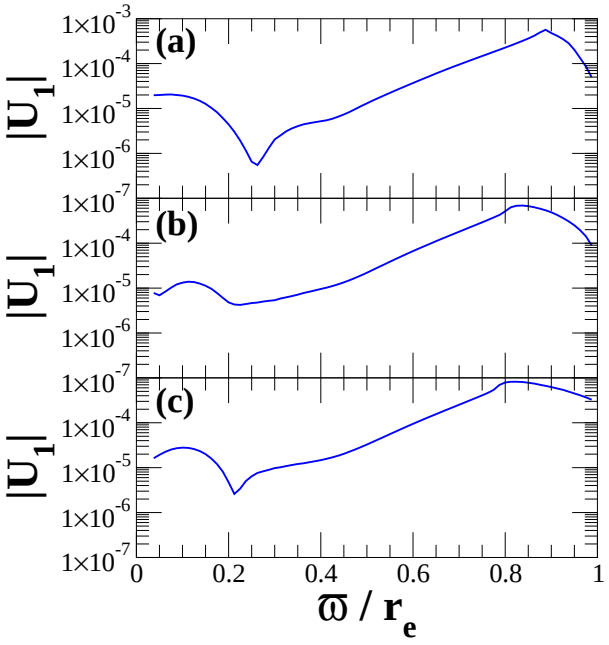

FIG. 4. Same as Fig. 3 but for $m = 1$. Note that U_1 represent the $m = 1$ scalar potential density-weighted average in the equatorial plane. The labels (a), (b), and (c) denote the evolution time $t = 52.0\ P_c$, $58.5\ P_c$, and $64.9\ P_c$, respectively. We find features similar to the cylindrical model (Fig. 2) in which no nodes are present.

urates its amplitude around $M_2 \approx 0.16$ for model I and $M_1 \approx 0.006$ for model II. Note that P_c is the central rotation period of the equilibrium star. The diagnostic M_1 and M_2 clearly show that the characteristic frequency is $\Re[\omega] = 0.387\ \Omega_c$ for model I and $\Re[\omega] = 0.586\ \Omega_c$ for model II, and the growth timescale is $\tau \equiv (\Im[\omega_i])^{-1} = 10.7\ P_c$ for model I and $\tau \equiv (\Im[\omega_i])^{-1} = 9.75\ P_c$ for model II, both timescales being extracted from the first $60\ P_c$. Note that our timescales are typical for low T/W dynamical instability [35]. We extract the complex frequencies by spectrum analysis [29] for the real part and the fitting formula of the dominant m mode of M_1 and M_2 diagnostics for the imaginary part. Note that 161 grid points are covered along the equatorial diameter of the star, with an equatorial radius twice as large as the outer boundary for each coordinate direction. We also check the different grid resolution for accuracy in both characteristic frequencies and growth timescales. We find that the characteristic frequency changes 0.4%–2% in the relative error rate and the growth timescale changes 20%–40%, the covered grid points along the equatorial diameter of the star varying between 121 and 161, fixing the ratio between the stellar radius and the outer boundary.

The real part of the eigenfrequency in the cylindrical model roughly agrees with that of hydrodynamical simulation. This situation is improved to $\Re[\omega] = 0.352\ \Omega_c$ and $\Im[\omega] = 0.0168\ \Omega_c$ for model I, $m = 2$, $N = 0$, when we take the z structure of δU_m and $\delta\Phi_m$ into account as associated Legendre polynomial functions $P_m^m(z)$. However, the imaginary part of the eigenfrequency, which represents the growth timescale of the instability, has few times difference with that of hydrodynamic simulation. This may be the fact that rotational configuration of the stars is not fully taken into account in our model. The results of quasinormal modes of black holes suggest that the imaginary part of eigenfrequency decreases as the black hole rotation becomes fast for corotating modes [36]. Therefore, two-dimensional eigenvalue analysis of differentially rotating stars is required for the full agreement of complex eigenfrequency with corotation, but this, however, is out of the scope of this paper.

We also compute the $m = 1$ and $m = 2$ diagnostic of scalar potential density-weighted average U_m in the area of equatorial plane as

$$U_m = \frac{1}{U}\int_S ds\ ue^{im\varphi}, \qquad U = \int_S ds\ u,$$

where $u \equiv H + \Phi = \varepsilon + P/\rho + \Phi$ and ε is the specific internal energy. The diagnostics U_1 and U_2 are regarded as "eigenfunction" when the system possesses a dominant characteristic frequency and growth timescale, as it is regarded as a "single" mode. Our choice of low T/W dynamically unstable star clearly meets this criteria. We show our eigenfunction in the equatorial plane computed from hydrodynamic simulation in Figs. 3 and 4. The slope of the $m = 2$ eigenfunction seems to have a sharp change in model I around the radius $\varpi/r_e \approx 0.45$ for all

three snapshots. The $m = 1$ eigenfunction seems to have a sharp change in model II around $\varpi/r_e \approx 0.20$ for all three snapshots. Although hydrodynamics system may contain multiple "modes" in the nonlinear regime, and they complicate the outcome, we find similar behavior in the diagnostics as what is found in the eigenfunction by linear analysis.

V. CONCLUSIONS

We have investigated the unstable feature of low T/W dynamical instabilities in differentially rotating stars by means of normal mode analysis in the equatorial plane.

We find unstable normal modes for low T/W dynamically unstable stars in the linear analysis. Any additional modes to the well-known f and p modes in the linear analysis are not found in our analysis, and these modes become unstable when corotation radii exist inside the stars. The frequencies of the real part in the cylindrical model of the linear analysis roughly agree with those of hydrodynamic simulation. The results confirm that our models are efficient for finding low T/W dynamically unstable stars.

We also find that the eigenfunction of the modes have a similar behavior to the well-known f and p modes. Once corotation exists inside the stars, the perturbed enthalpy oscillates between corotation and the surface radius. Note that the perturbed enthalpy globally oscillates between the center and the surface for the no-corotation case. This may indicate that the perturbed enthalpy is affected by corotation singularity barrier, and therefore cannot cross the corotation radius. This feature requires reinterpretation of the pulsation modes in rotating stars when corotation exists inside the stars.

We have computed the linear analysis in the equatorial plane by reducing the system to ordinary differential equations. Our results clearly show that rotational configuration of the star should be fully taken into account for quantitative comparison to hydrodynamic simulations. To make a complete agreement between the linear analysis and hydrodynamic simulation, a two-dimensional eigenmode analysis with corotation is required, and it is a challenging task in this field.

ACKNOWLEDGMENTS

It is our pleasure to thank Toni Font for valuable suggestions about the shock capturing scheme to install in our hydrodynamic code. This work was supported in part by JSPS Grant-in-Aid for Young Scientists B (Grant No. 201103201) and the Waseda University Grant for Special Research Projects (Grant No. 2013A-6164). Numerical computations were performed on the Cray XC30 cluster in the center for Computational Astrophysics, National Astronomical Observatory of Japan, and on the cluster at Relativistic Astrophysics Group at Department of Science, Waseda University.

[1] B. K. Pickett, R. H. Durisen, and G. A. Davis, Astrophys. J. **458**, 714 (1996).
[2] J. M. centerlla, K. C. B. New, L. L. Lowe, and J. D. Brown, Astrophys. J. **550**, L193 (2001).
[3] M. Shibata, S. Karino, and Y. Eriguchi, Mon. Not. R. Astron. Soc. **334**, L27 (2002).
[4] M. Shibata, S. Karino, and Y. Eriguchi, Mon. Not. R. Astron. Soc. **343**, 619 (2003).
[5] M. Saijo, T. W. Baumgarte, and S. L. Shapiro, Astrophys. J. **595**, 352 (2003).
[6] S. Chandrasekhar, *Ellipsoidal Figures of Equilibrium*, (Yale University, New Haven, CT, 1969), Chap. 5.
[7] J. Tassoul, *Theory of Rotating Stars*, (Princeton University, Princeton, NJ, 1978), Chap. 10.
[8] S. L. Shapiro and S. A. Teukolsky, *Black Holes, White Dwarfs, and Neutron Stars*, (Wiley, New York, 1983), Chap. 7.5.
[9] V. Paschalidis, W. E. East, F. Pretorius, and S. L. Shapiro, Phys. Rev. D**92**, 121502 (2015).
[10] W. E. East, V. Paschalidis, F. Pretorius, and S. L. Shapiro, Phys. Rev. D**93**, 024011 (2016).
[11] T. Kuroda, T. Takiwaki, and K. Kotake, Phys. Rev. D**89**, 044011 (2014).
[12] B. Zink, N. Stergioulas, I. Hawke, C. D. Ott, E. Schnetter, and E. Müller, Phys. Rev. Lett. **96**, 161101 (2006).
[13] B. Zink, N. Stergioulas, I. Hawke, C. D. Ott, E. Schnetter, and E. Müller, Phys. Rev. D**76**, 024019 (2007).
[14] C. Reisswig, C. D. Ott, E. Abdikamalov, R. Haas, P. Mösta, and E. Schnetter, Phys. Rev. Lett. **111**, 151101 (2013).
[15] N. Andersson *et al.*, Classical Quantum Gravity **30**, 193002 (2013).
[16] E. Balbinski, Mon. Not. R. Astron. Soc. **216**, 897 (1985).
[17] J. C. B. Papaloizou and J. E. Pringle, Mon. Not. R. Astron. Soc. **225**, 267 (1987).
[18] D. Tsang and D. Lai, Mon. Not. R. Astron. Soc. **387**, 446 (2008).
[19] A. L. Watts, N. Andersson, and D. I. Jones, Astrophys. J. Lett. **618**, L37 (2005).
[20] M. Saijo and S.'i. Yoshida, Mon. Not. R. Astron. Soc. **368**, 1429 (2006).
[21] S. Ou and J. E. Tohline, Astrophys. J. **651**, 1068 (2006).
[22] A. Passamonti and N. Andersson, Mon. Not. R. Astron. Soc. **446**, 555 (2015).
[23] J. R. Ipser and L. Lindblom, Phys. Rev. Lett. **62**, 2777 (1989).
[24] F. Lignières, M. Rieutord, and D. Reese, Astron. Astrophys. **455**, 607 (2006).
[25] D. R. Reese, K. B. MacGregor, S. Jackson, A. Skumanich, and T. S. Metcalfe, Astron. Astrophys. **506**, 189 (2009)
[26] R.-M. Ouazzani, M.-A. Dupret, and D. R. Reese, Astron. Astrophys. **547**, A75 (2012).
[27] S. Karino and Y. Eriguchi, Astrophys. J. **592**, 1119

(2003).
[28] I. Hachisu, Astrophys. J. Suppl. **61**, 479 (1986).
[29] M. Saijo and Y. Kojima, Phys. Rev. D**77**, 063002 (2008).
[30] J. R. Ipser and L. Lindblom, Astrophys. J. **355**, 226 (1990).
[31] J. P. Cox, *Theory of Stellar Pulsation*, (Prinston University, Prinston, NJ, 1980), Chap. III, Sec. 17.
[32] W. Unno, Y. Osaki, H. Ando, H. Saio, and H. Shibahashi, *Nonradial Oscillations of Stars*, (University of Tokyo, Tokyo, 1989), Chap. III, Sec. 14.
[33] E. F. Toro, *Riemann Solvers and Numerical Methods for Fluid Dynamics*, (Springer, New York, 2009), Chap. 10.
[34] R. J. LeVeque, D. Mihalas, E. A. Dorfi, and E. Muller, *Computational Methods for Astrophysical Fluid Flow*, (Springer, Berlin, 1998), Chap. 4.7.
[35] C. D. Muhlberger, F. H. Nouri, M. D. Duez, F. Foucart, L. E. Kidder, C. D. Ott, M. A. Scheel, B. Szilágyi, and S. A. Teukolsky, Phys. Rev. D**90**, 104014 (2014).
[36] E. W. Leaver, Proc. R. Soc. A **402**, 285 (1985).